Journal of Power Sources 265 (2014) 104–109

Contents lists available at ScienceDirect

Journal of Power Sources

journal homepage: www.elsevier.com/locate/jpowsour

Nano-$Li_3V_2(PO_4)_3$ enwrapped into reduced graphene oxide sheets for lithium-ion batteries

Bin Cheng, Xu-Dong Zhang, Xiao-Hang Ma, Jian-Wu Wen, Yan Yu, Chun-Hua Chen*

CAS Key Laboratory of Materials for Energy Conversions, Department of Materials Science and Engineering & Collaborative Innovation Center of Suzhou Nano Science and Technology, University of Science and Technology of China, Anhui, Hefei 230026, China

HIGHLIGHTS

- Nano-$Li_3V_2(PO_4)_3$ enwrapped into rGO sheets is synthesized.
- Liquid nitrogen was used as a coolant in the freeze-drying method.
- The material shows excellent rate performance in lithium ion batteries.

ARTICLE INFO

Article history:
Received 29 January 2014
Received in revised form
21 March 2014
Accepted 11 April 2014
Available online 4 May 2014

Keywords:
Lithium vanadium phosphate
Reduced graphene oxide
Freeze-drying
Liquid nitrogen
Rate performance
Lithium ion batteries

ABSTRACT

Liquid nitrogen was used as a coolant in the freeze-drying method to synthesize nano-$Li_3V_2(PO_4)_3$/reduced graphene oxide ($LVPG_N$) for the first time. In this material, reduced graphene oxide (rGO) (6.6 wt % in content) formed a 3D-framework and $Li_3V_2(PO_4)_3$ nanoparticles (30–150 nm) were strongly adhered to the surface of the rGO and enwrapped into the rGO sheets uniformly. The LVP nanoparticles can decrease the lithium ion diffusion length and the rGO can effectively improve the electronic conductivity. The material shows great rate performance with a capacity of 105.7 mAh g^{-1} at 20C for 3.0–4.3 V, and a good cycling performance with a discharge capacity of 123.2 mAh g^{-1} (96.7% of the first discharge capacity 127.4 mAh g^{-1}) after 100 cycles at 0.1C.

1. Introduction

In recent years, lithium ion batteries (LIBs) are widely considered as a better choice for the next generation of plug-in hybrid electric vehicles due to their higher energy densities and power densities than other energy storage systems [1]. Among all the cathode materials, monoclinic lithium vanadium phosphate $Li_3V_2(PO_4)_3$ (LVP) has been regarded as a promising candidate with good ionic mobility, excellent cycling capability and stability [2,3]. However, just like $LiFePO_4$, LVP suffers from a low intrinsic electronic conductivity [4] (10^{-8} S cm^{-1}), which strongly limits its rate performance. This problem can be partly solved by reducing the particle size [5], doping with other metals [6,7], and coating with an electronically conductive material [8–10], such as carbon.

Compared with traditional carbon, graphene or reduced graphene oxide (rGO), is an effective conductive additive for LIBs owing to its high electrical conductivity and high specific surface area. Some electrode materials, such as $LiFePO_4$ [11], $Li_3V_2(PO_4)_3$ [12], and Fe_3O_4 [13], have been successfully incorporated with graphene/rGO to achieve greatly improved electrochemical performances.

Freeze-drying method is a classical technique which has been used to synthesize several cathode materials, such as $LiCoO_2$ [14], $LiFePO_4$ [15,16], $LiNi_{0.5}Mn_{0.5}O_2$ [17], LiV_3O_8 [18], and so on. The superiority of freeze-drying method is to construct porous nanoscale structures of materials [16,19]. Herein, we introduce liquid nitrogen as a coolant to freeze the precursor followed by steps of freeze-drying and heat treatment to synthesize nano-$Li_3V_2(PO_4)_3$/reduced grapheme oxide ($LVPG_N$). Such an rGO-wrapped electrode material is found to exhibit high specific capacity at high current densities, namely much improved high rate capability.

* Corresponding author. Tel.: +86 551 63606971; fax: +86 551 63601592.
E-mail address: cchchen@ustc.edu.cn (C.-H. Chen).

http://dx.doi.org/10.1016/j.jpowsour.2014.04.046
0378-7753/

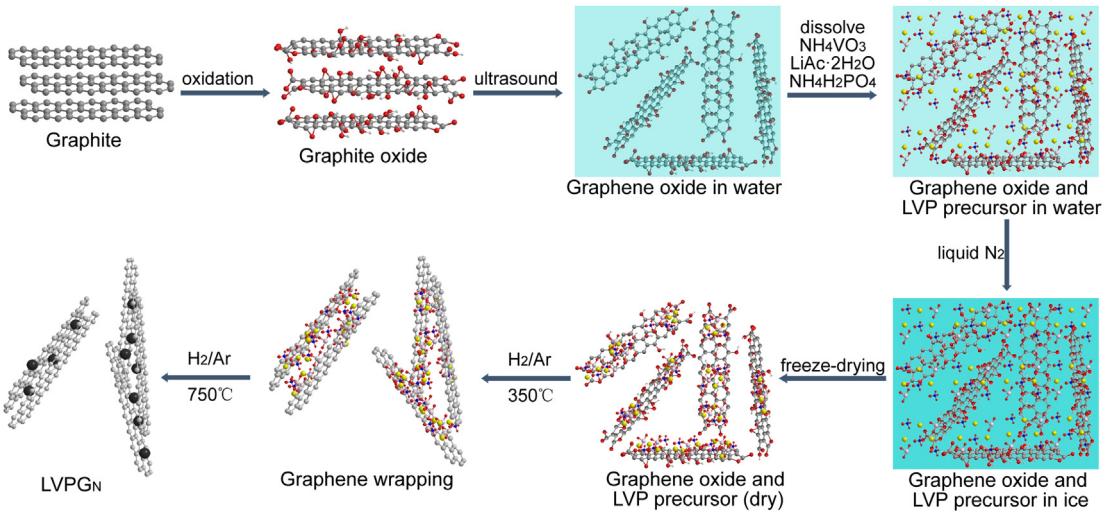

Fig. 1. Scheme for the formation of $LVPG_N$ composite.

2. Experimental

2.1. Synthesis of nano-$Li_3V_2(PO_4)_3$/reduced grapheme oxide ($LVPG_N$)

As showed in Fig. 1, first, graphite oxide was prepared from natural graphite by a Hummers method. [20] To obtain a graphene oxide (GO) solution (10 mg mL^{-1}), the obtained graphite oxide was dispersed in water and ultrasonicated for 2 h. Then, NH_4VO_3 (2 mmol), oxalic acid (4 mmol), $NH_4H_2PO_4$ (3 mmol), $LiAc{\cdot}2H_2O$ (3.15 mmol) were dissolved sequentially in the GO solution (10 mL) and slightly heated at about 50 °C to promote dissolution. The mixture was well stirred for 30 min and rapidly frozen in liquid nitrogen followed by freeze-drying to obtain a dry precursor. The precursor was grounded and preheated at 350 °C in 5% H_2/Ar atmosphere for 5 h to expel H_2O, CO_2, and NH_3. After cooling to room temperature, the resulted powder was grounded and sintered at 750 °C for 8 h under a flowing H_2/Ar to obtain the nano-$Li_3V_2(PO_4)_3$/reduced graphene oxide ($LVPG_N$) composite.

For comparison, two samples micro-$Li_3V_2(PO_4)_3$/reduced graphene oxide (LVPG) and micro-$Li_3V_2(PO_4)_3$/C (LVPC) were prepared. LVPG was prepared following a procedure that was almost the same as for $LVPG_N$ but replaced the liquid nitrogen process by a slow freezing step in fridge. Moreover, LVPC was prepared through a sol–gel method reported in our previous paper [21].

2.2. Materials characterization

The crystalline structures of the final powders were analyzed by X-ray diffraction (XRD) using a diffractometer (Philips X'Pert Pro Super, Cu Kα radiation) in the 2θ range of 10–60°. Raman spectra were taken by a RAMAMLOG 6 (Spex, USA) with a 50× objective lens and 514.5 nm laser excitation. Thermogravimetric analysis (TGA) of the composites was conducted in air at a heating rate of 10 °C min^{-1} from 30 °C to 750 °C using a thermal analyzer (TGA50H). The morphology was observed under a scanning electron microscope (SEM, JSM-6390LA) and the surface composition was analyzed by energy dispersive spectroscopy (EDS, JED-2300). The nanostructure was examined using a

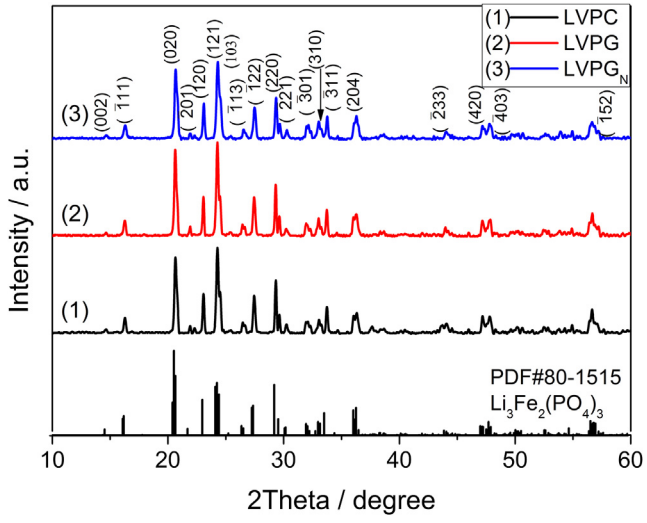

Fig. 2. XRD patterns of LVPC, LVPG, and $LVPG_N$ composites.

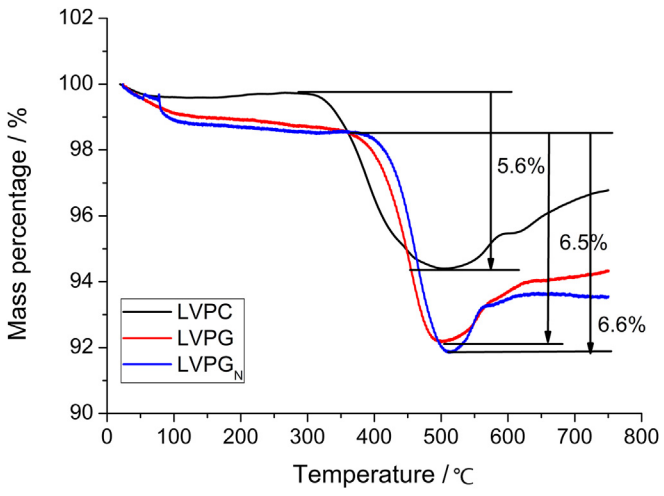

Fig. 3. TGA curves of LVPC, LVPG, and $LVPG_N$ composites.

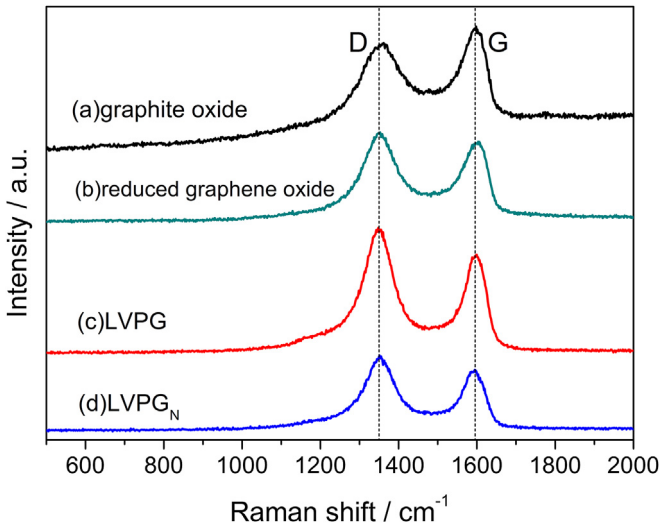

Fig. 4. Raman spectra of graphite oxide (a), rGO reduced by hydrazine hydrate (b), LVPG (c), and LVPG$_N$ (d).

high-resolution transmission electron microscope (HRTEM, JEOL-2010).

2.3. Electrochemical measurements

The electrochemical characterizations of these three samples were evaluated using CR2032 coin cells. An electrode laminate was prepared by mixing 80wt% active materials (LVP), 10wt% acetylene black (AB) and 10wt% poly(vinylidene difluoride) (PVDF) in NMP to form a homogeneous slurry, which was uniformly coated on an aluminum foil with a doctor-blade. The laminate was dried at 120 °C for several hours in an electric oven. Then CR2032 coin-type half-cells LVPG$_N$ vs. Li were assembled in an argon-filled glove box (MBRAUN LABMASTER 130) with both the moisture content and oxygen levels less than 1 ppm. In the half-cells, the mass loading of cathode materials was about 2 mg cm^{-2} and a metallic lithium foil served as the anode. The electrolyte was 1 M $LiPF_6$ in ethylene carbonate (EC)/dimethyl carbonate (DMC) (1:1 in volume), while a polypropylene micro-porous film (Celgard 2300) was used as the separator. The cells were tested on a NEWWARE BTS-610 multi-channel battery test system at different current densities in voltage ranges of 3.0–4.3 V. Electrochemical impedance spectroscopy (EIS) measurements were performed on a CHI660d electrochemical workstation over a frequency range from 0.01 Hz to 100 kHz with the AC amplitude of 5.0 mV. The half cells with different cathode materials were discharged to about 4.0 V after one cycle activation and once more charge step.

3. Results and discussion

The XRD patterns of the as-synthesized composites (Fig. 2) indicate that all the diffraction peaks can be indexed well to the monoclinic $Li_3V_2(PO_4)_3$ with the space group $P2_1/n$, that is very close to the pattern of $Li_3Fe_2(PO_4)_3$ (JCPDS: 80-1515). No obvious peaks of impurities can be observed, and, due probably to the low content of rGO, no peaks related to rGO can be detected.

The carbon content of the composites is revealed by thermogravimetric analysis shown in Fig. 3. According to Rui et al. [3], the composites initially undergo a weight loss in the temperature range of 300–500 °C, which is attributed to the removal of carbon by its oxidation into gaseous product (CO or CO_2). And then above 500 °C, LVP gains weight due to the oxidation of V(III) to higher valence states in air. According to the weight loss step on the TGA curves, the carbon content of LVPC, LVPG, LVPG$_N$ are 5.6%, 6.5%, 6.6%, respectively.

Fig. 4 shows the Raman spectra of graphite oxide (Fig. 4a), reduced graphene oxide reduced by hydrazine hydrate (Fig. 4b), LVPG (Fig. 4c), LVPG$_N$ (Fig. 4d). All the spectra displays two characteristic bands of carbonaceous materials located at 1363 cm^{-1} (D-

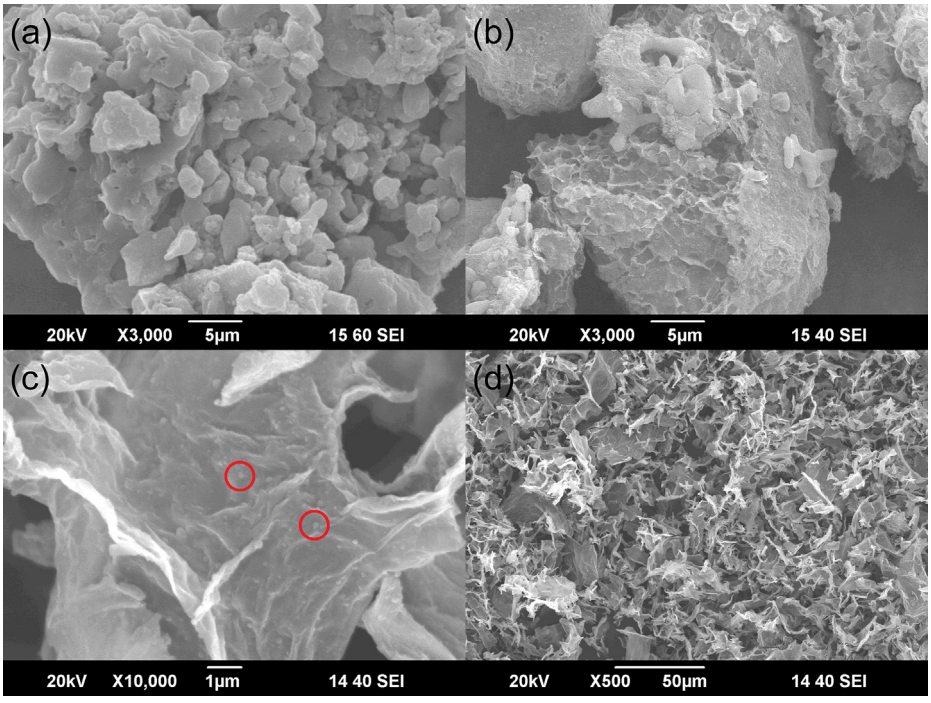

Fig. 5. SEM images of LVPC (a), LVPG (b), LVPG$_N$ (c), and the panoramic view of LVPG$_N$ (d).

Table 1
The EDS analysis of different areas on the surface of $LVPG_N$.

	C	O	P	V	Au
Atom/%					
001	64.48	23.19	6.32	5.07	0.94
002	64.24	24.99	6.13	3.93	0.70
003	56.73	32.15	6.10	3.94	1.08
004	62.08	27.18	5.72	4.15	0.88
Mass/%					
001	43.40	20.78	10.97	14.48	10.37
002	45.40	23.53	11.18	11.79	8.11
003	37.91	28.62	10.51	11.15	11.82
004	42.82	24.97	10.18	12.13	9.90

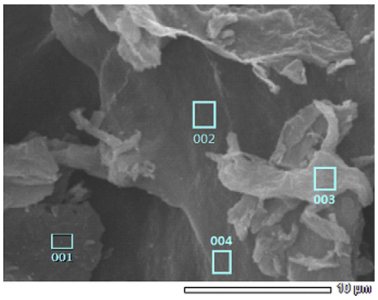

band, disorder-induced phonon mode) and at 1595 cm^{-1} (G-band, graphite band). The I_D/I_G intensity ratio are 1.45 for rGO reduced by hydrazine hydrate (Fig. 4b), 1.62 for LVPG (Fig. 4c), 1.62 for $LVPG_N$ (Fig. 4d), indicating the formation of 3D porous graphene networks in LVPG and $LVPG_N$.

The SEM images of LVPC, LVPG, $LVPG_N$ composites are shown in Fig. 5. LVPC particles are particles with an average size of 1–3 μm in Fig. 5a. In Fig. 5b, we can find that rGO sheets coagulate together building up large particles and some seemingly micro-LVP particles lie on the surface of the rGO sheets. As to $LVPG_N$ in Fig. 5c (detail) and Fig. 5d (panoramic view), there seem to be only rGO sheets with very few LVP nanoparticles distributing on the rGO sheets as circled in the image. But this small amount of LVP particles does not match the mass ratio of 93.4%, so we imagine that the major portion of LVP is either adhered to the surface of rGO uniformly or enwrapped into the rGO sheets.

To determine which above case is true, energy dispersive spectroscopy (EDS) technique was used for the elemental analysis and the results are shown in Table 1. If we compare the EDS results of area 001 (surface plus a particle) and areas 002 and 004 (smooth surface), the contents of carbon are all around 43–45 wt%, indicating that the visible LVP particles are not the major presence status of LVP ingredient. And we can find that at different areas, the total mass ratio of *P* and *V* is approximately 22 wt% while the carbon ratio is more than 40 wt%. We can thus deduce that a predominant portion of LVP particles are enwrapped into the rGO sheets. It is also noticed that the P:V ratio for area 001 and C content show some deviations from the other areas, which may

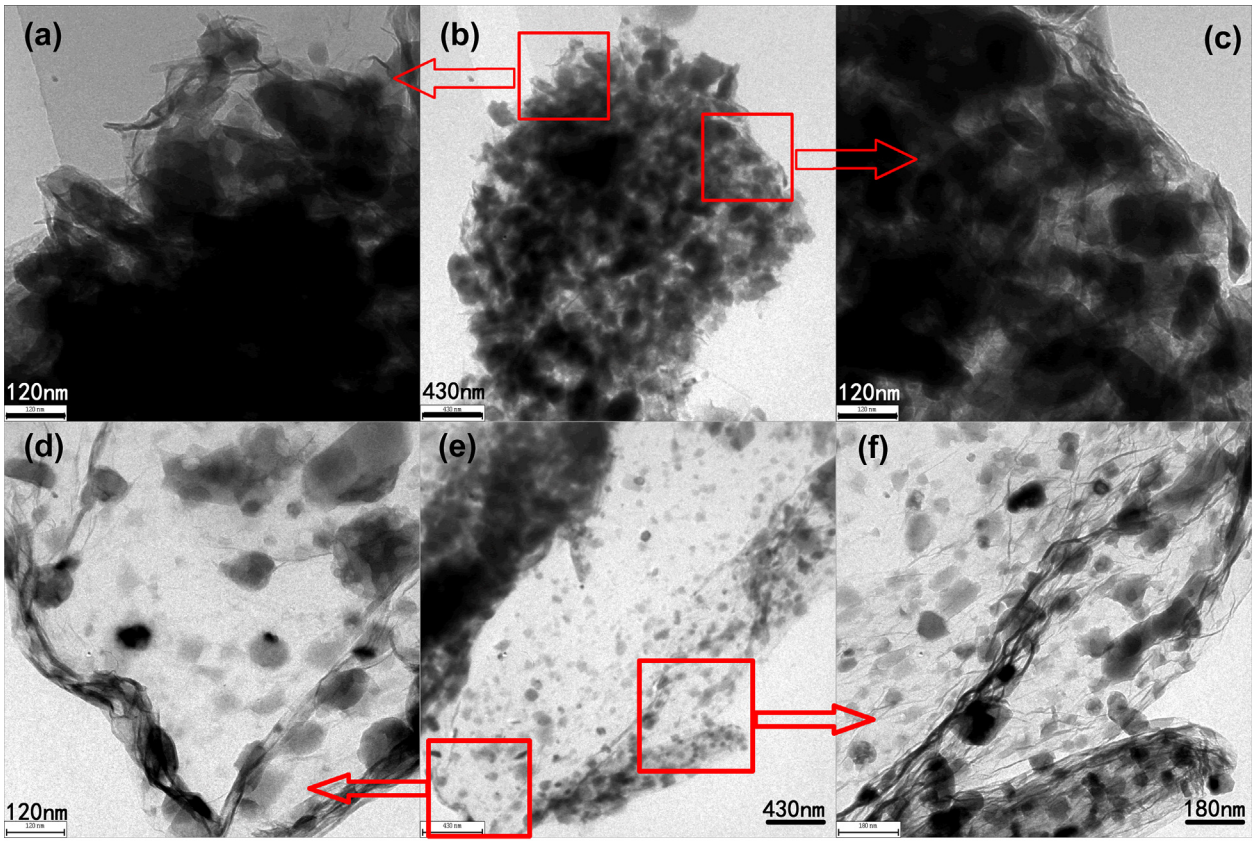

Fig. 6. TEM images of LVPG (a–c) and $LVPG_N$ (d–f).

suggest a small extent of inhomogeneity of the sample. Nevertheless, both the results of XRD analysis (Fig. 2) and other values in Table 1 indicate that the composition of the sample is predominantly $Li_3V_2(PO_4)_3$.

We can see more clearly the morphology of LVPG and $LVPG_N$ in the TEM image shown in Fig. 6. Obviously, the rGO sheets coagulate together in LVPG (Fig. 6b) but those in $LVPG_N$ (Fig. 6e) are separated. As shown in Fig. 6d–f, LVP particles with size of 30–150 nm are adhered to the surface of rGO and enwrapped inside. But the LVP particles in LVPG are much larger.

To understand the formation of such a special morphology, we take into consider the scheme for the formation of $LVPG_N$ as shown in Fig. 1. First, after dissolving the starting materials into the GO solution, its rapid solidification by liquid nitrogen can prevent the segregation of different salts from the solution to crystallize. On the other hand, the slow freezing in fridge for LVPG cannot effectively prevent from the segregation, so there are many micron-size particles in LVPG (Fig. 5b) but none in $LVPG_N$ (Fig. 5c and Fig. 6d–f). Second, the freeze-drying method, compared with hot-drying, can preclude the rGO sheets from reuniting with each other to provide more specific surface area to accommodate the LVP precursor. Also, the heat treatment is accompanied with the simultaneous reductions of both vanadium (V) into vanadium (III) in LVP and graphene oxide (GO) into rGO. With the proceeding of the GO reduction and thus the decrease in oxygen content in rGO, the surface energy of rGO becomes smaller and smaller [22], which can cause the bending of graphene sheets and wrapping of the LVP precursors. Eventually, while the wrapped precursors react with one another to generate LVP nanoparticles, the wrinkled structure of rGO sheets can block the paths for transporting ions and the

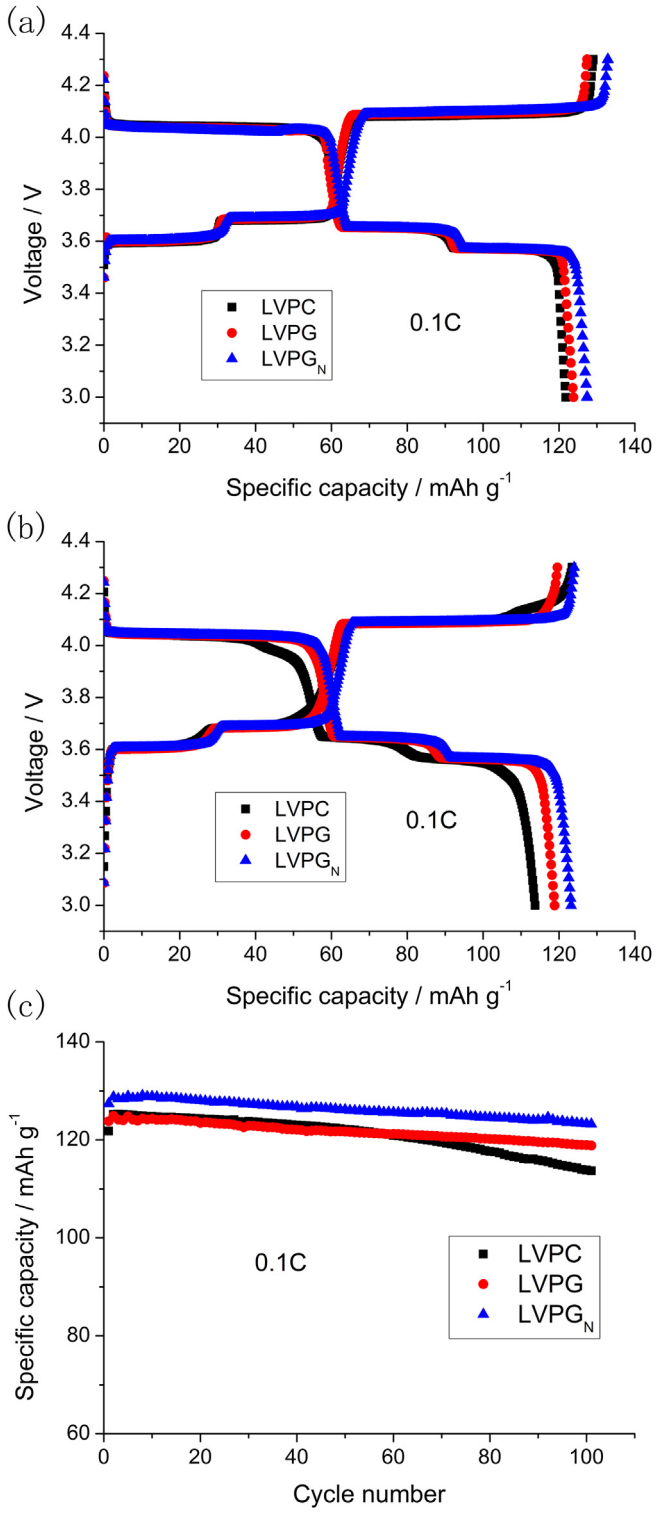

Fig. 7. Cycling performance of LVPC, LPVG, $LVPG_N$: the voltage profiles of 1st cycle (a) and 100th cycle (b) at 0.1C in the voltage range of 3.0–4.3 V, and their cycling performance at 0.1C (c).

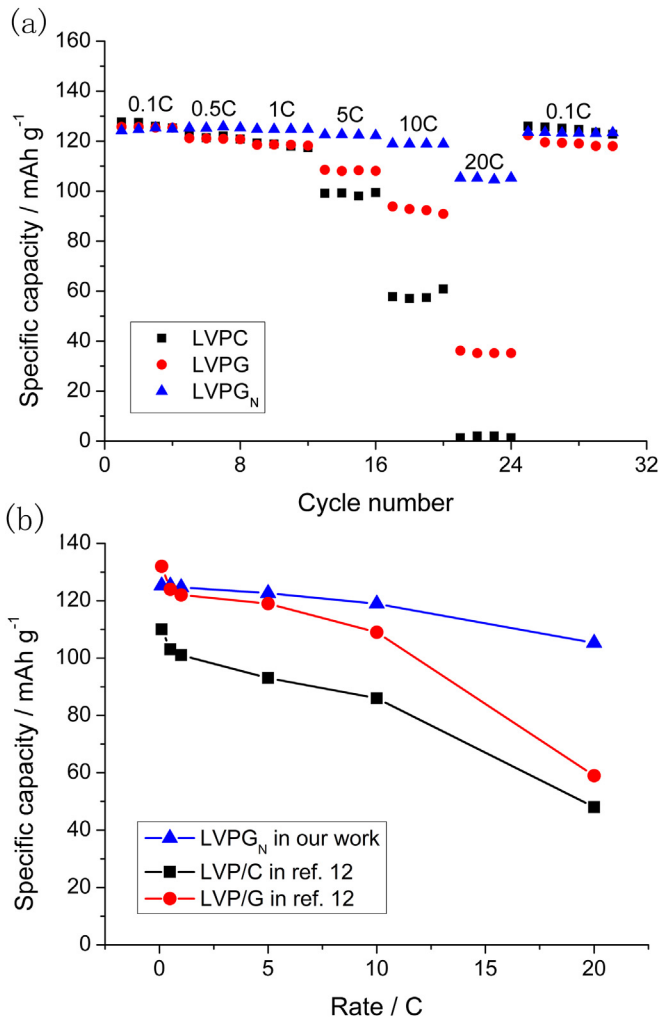

Fig. 8. Rate performance of LVPC, LPVG, $LVPG_N$ from 0.1C to 20C (a) and the comparison with Ref. [12] (b).

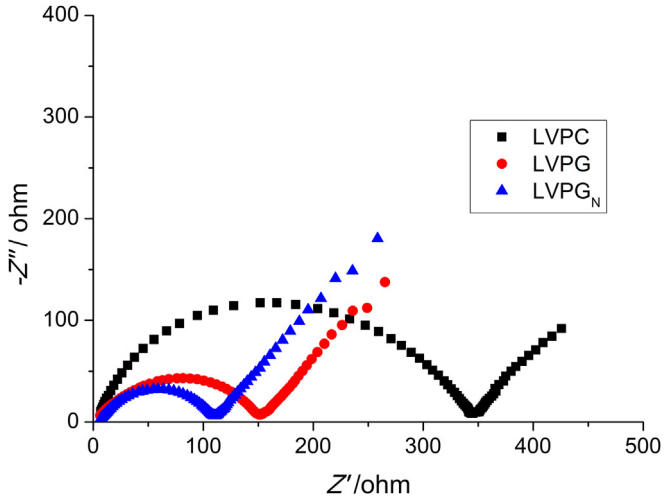

Fig. 9. Electrochemical impedance spectra (EIS) measurement. The half cells with different cathode materials were discharged to about 4.0 V after one cycle activation and once more charge step.

crystals cannot grow. Because of these, the majority of LVP particles maintain a size of less than 100 nm.

With nano LVP particles enwrapped into rGO sheets, $LVPG_N$ material is expected to have excellent electrochemical performance (Fig. 7 and Fig. 8). Fig. 7a and b shows the voltage profiles of first and 100th cycle. It can be shown clearly that the lithium extraction–insertion processes are very reversible so that their capacities fade slightly after 100 cycles. It is found in Fig. 7a–c that LVPC, LVPG, $LVPG_N$ deliver a first discharge capacities of 121.8, 123.8, and 127.4 mAh g^{-1}, respectively. After 100 cycles, the discharge capacities are 113.7, 118.8, 123.2 mAh g^{-1} with capacity retentions of 93.3%, 96.0%, 96.7%, suggesting that the synthesized materials exhibit excellent cyclability.

Fig. 8 shows the rate capability of the three comparative LVP materials. It can be seen that $LVPG_N$ electrode delivers discharge capacities of 125.3, 125.2, 124.7, 122.6, 118.9, 105.2 mAh g^{-1} at 0.1C, 0.5C, 1C, 5C, 10C, 20C, respectively. This rate capability is much better than that of LVPC and LVPG, whose specific capacities are 57.7, 93.8 mAh g^{-1} at 10C and 2.0, 36.1 mAh g^{-1} at 20C, respectively. Comparing the rate performance of $LVPG_N$ with the LVP/graphene synthesized in other works [12] (Fig. 8b), one can find that at the high rates of 10C and 20C, the specific capacities of $LVPG_N$ are much higher than those in Ref. [12]. This great rate performance can be ascribed to the short lithium ion transport path in nano-$Li_3V_2(PO_4)_3$ particles and the rGO which can provide a fast electron conduction. This interpretation is confirmed by the EIS measurement (Fig. 9). The half cells with different cathode materials were discharged to about 4.0 V after one cycle activation and once more charge step. As expected, the impedance component in $LVPG_N$ is much lower than those in LVPC and LVPG.

4. Conclusions

In summary nano-$Li_3V_2(PO_4)_3$ enwrapped into reduced grapheme oxide ($LVPG_N$) with much improved rate capability has been prepared through a freeze-drying method in which we used liquid nitrogen as a coolant for the first time. In the material, reduced graphene oxide (rGO) formed a 3D-framework and $Li_3V_2(PO_4)_3$ nanoparticles (30–150 nm) were strongly adhered to the surface of the rGO and enwrapped into the rGO sheets uniformly. The nanoparticles can decrease the lithium transport path and the rGO can effectively improve the electron conductivity. So this material represents a very great rate performance in lithium ion batteries. Freeze-drying method using liquid nitrogen as a coolant is proved to be an effective way to prepare nanoparticles.

Acknowledgments

This study was supported by National Natural Science Foundation of China (grant no. 20971117, 10979049, 21171015 and J1030412). We are also grateful to Elementec Ltd in Suzhou.

References

[1] B. Kang, G. Ceder, Nature 458 (2009) 190–193.
[2] H. Huang, S.C. Yin, T. Kerr, N. Taylor, L.F. Nazar, Adv. Mater. 14 (2002) 1525–1528.
[3] X.H. Rui, C. Li, C.H. Chen, Electrochim. Acta 54 (2009) 3374–3380.
[4] S.C. Yin, H. Grondey, P. Strobel, M. Anne, L.F. Nazar, J. Am. Chem. Soc. 125 (2003) 10402–10411.
[5] B. Pei, Z. Jiang, W. Zhang, Z. Yang, A. Manthiram, J. Power Sources 239 (2013) 475–482.
[6] R. Wang, S. Xiao, X. Li, J. Wang, H. Guo, F. Zhong, J. Alloys Compd. 575 (2013) 268–272.
[7] J. Yao, Z. Jia, P. Zhang, C. Shen, J. Wang, K.F. Aguey-Zinsou, C.A. Ma, L. Wang, Ceram. Int. 39 (2013) 2165–2170.
[8] L.L. Zhang, G. Peng, G. Liang, P.C. Zhang, Z.H. Wang, Y. Jiang, Y.H. Huang, H. Lin, Electrochim. Acta 90 (2013) 433–439.
[9] J. Zhu, R. Yang, K. Wu, Ionics 19 (2012) 577–580.
[10] X. Rui, D. Sim, K. Wong, J. Zhu, W. Liu, C. Xu, H. Tan, N. Xiao, H.H. Hng, T.M. Lim, Q. Yan, J. Power Sources 214 (2012) 171–177.
[11] J. Yang, J. Wang, D. Wang, X. Li, D. Geng, G. Liang, M. Gauthier, R. Li, X. Sun, J. Power Sources 208 (2012) 340–344.
[12] H. Liu, G. Yang, X. Zhang, P. Gao, L. Wang, J. Fang, J. Pinto, X. Jiang, J. Mater. Chem. 22 (2012) 11039.
[13] W. Chen, S. Li, C. Chen, L. Yan, Adv. Mater. 23 (2011) 5679–5683.
[14] O.A. Shlyakhtin, S.H. Choi, Y.S. Yoon, Y.J. Oh, Electrochim. Acta 50 (2004) 511–516.
[15] V. Palomares, A. Goñi, I.G. de Muro, I. de Meatza, M. Bengoechea, O. Miguel, T. Rojo, J. Power Sources 171 (2007) 879–885.
[16] X. Xi, G. Chen, Z. Nie, S. He, X. Pi, X. Zhu, J. Zhu, T. Zuo, J. Alloys Compd. 497 (2010) 377–379.
[17] O.A. Shlyakhtin, Y.S. Yoon, S.H. Choi, Y.J. Oh, Electrochim. Acta 50 (2004) 505–509.
[18] S. Huang, Y. Lu, T.Q. Wang, C.D. Gu, X.L. Wang, J.P. Tu, J. Power Sources 235 (2013) 256–264.
[19] X. Xin, X. Yao, Y. Zhang, Z. Liu, X. Xu, J. Solid State Electrochem. 16 (2012) 2733–2738.
[20] W.S. Hummers, R.E. Offemen, J. Am. Chem. Soc. 80 (1958) 1339.
[21] X.H. Rui, C. Li, J. Liu, T. Cheng, C.H. Chen, Electrochim. Acta 55 (2010) 6761–6767.
[22] S. Wang, Y. Zhang, N. Abidi, L. Cabrales, Langmuir 25 (2009) 11078–11081.